Direct measurements of deglacial monsoon strength in a Chinese stalagmite

Ian J. Orland[1,2]*, R. Lawrence Edwards[1], Hai Cheng[1,3], Reinhard Kozdon[2,4], Mellissa Cross[1], and John W. Valley[2]
[1]Department of Earth Sciences, University of Minnesota, 310 Pillsbury Drive SE, Minneapolis, Minnesota 55455, USA
[2]WiscSIMS (Wisconsin Secondary Ion Mass Spectrometer Laboratory), Department of Geoscience, University of Wisconsin, 1215 West Dayton Street, Madison, Wisconsin 53706, USA
[3]Institute of Global Environmental Change, Xi'an Jiaotong University, Xi'an 710049, China
[4]Department of Marine and Coastal Sciences, Rutgers University, 71 Dudley Road, New Brunswick, New Jersey 08901, USA

ABSTRACT

Chinese speleothems (cave deposits) preserve a remarkable paleoclimate record in their oxygen isotope ratios ($\delta^{18}O$); the precise interpretation of this record has been the subject of stimulating discussion. Most studies link the $\delta^{18}O$ variability in Chinese speleothems to regional summer monsoon rainfall and/or rainfall integrated between tropical sources and cave sites. Discussion has centered on mechanisms behind this link as well as the location and seasonality of hypothesized rainfall changes. Until now, these hypotheses were not directly tested in speleothems because conventional drill sampling techniques are insufficient for measuring speleothem $\delta^{18}O$ at seasonal resolution. Here we use an ion microprobe to analyze seasonal $\delta^{18}O$ variability in an annually banded stalagmite from Kulishu Cave (northeastern China) that grew during the last deglaciation. The new seasonal resolution data show that the stalagmite $\delta^{18}O$ values record two aspects of regional monsoon dynamics: (1) changes in the isotopic fractionation of water vapor sourced from both the Indian and Pacific Oceans, and (2) the annual proportion of summer monsoon rainfall, which was systematically greater during the Holocene and Bølling-Allerød than during the Younger Dryas. Both relate to regional rainfall; the isotopic fractionation changes also relate to rainfall integrated from tropical sources.

INTRODUCTION

Speleothem $\delta^{18}O$ profiles from many locations in China follow the inverted signal of Northern Hemisphere summer insolation and record the millennial interstadial events observed in Greenland ice cores (Wang et al., 2001, 2008; Yuan et al., 2004; Dykoski et al., 2005; Kelly et al., 2006; Cheng et al., 2009, 2012a, 2012b). For a majority of the records, speleothems are sampled by conventional drilling techniques (0.5 mm spot drilling) whereby individual drill spots average $\delta^{18}O$ from multiple years of growth. Beginning with one of the earliest of these speleothem records (Wang et al., 2001), the $\delta^{18}O$ variability is interpreted as a proxy for East Asian Summer Monsoon (EASM) intensity. The interpretation is explained in two ways.

In the first explanation (Wang et al., 2001; Cheng et al., 2009; herein called the Wang-Cheng interpretation), speleothem $\delta^{18}O$ variability reflects a mixing model with two seasonal precipitation components; one is low $\delta^{18}O$ summer (monsoon) rainfall and the other is high $\delta^{18}O$ winter and spring rainfall. In this model, the annual fraction of monsoon rainfall dictates the drill sample $\delta^{18}O$ values. When boreal summer insolation is high, the EASM strengthens, leading to an increase in the annual proportion of low $\delta^{18}O$ monsoon rainfall, and so the drill sample $\delta^{18}O$ value is relatively low.

The second explanation proposes that the $\delta^{18}O$ of Chinese precipitation is dictated by Rayleigh-type fractionation of water vapor originating from Indian Ocean and Pacific Ocean sources (Yuan et al., 2004; herein referred to as the Yuan interpretation). In this model, increased summer insolation leads to an increase of upstream rainfall from air masses destined for Chinese cave sites, which ultimately results in lower $\delta^{18}O$(rain) values at the sites. This explanation can also be framed in terms of a mixing model with two seasonal precipitation components, but in this version the $\delta^{18}O$ of summer monsoon precipitation is the key variable that changes.

The two hypotheses have somewhat different climatic implications. In the Wang-Cheng explanation, speleothem $\delta^{18}O$ values respond directly to changes in the amount of summer monsoon rainfall at the cave site. In the Yuan interpretation, $\delta^{18}O$ changes relate to changes in the integrated amount of monsoon rainfall from tropical ocean sources to cave sites. By comparison, the model results of Pausata et al. (2011) suggest that $\delta^{18}O$ changes in Chinese speleothems result solely from changes in the amount of summer rainfall sourced from the Indian Ocean, explicitly ruling out analogous changes over the Pacific. Here we test to what extent each hypothesis explains the $\delta^{18}O$ record of stalagmite sample BW-1 (14.0–10.4 k.y. before present, A.D. 1950) from Kulishu Cave, China (39.7°N, 115.7°E, 610 m above sea level; Fig. 1), using an ion microprobe to perform 10-µm-diameter, seasonal resolution $\delta^{18}O$ analyses.

SAMPLE SELECTION

Sample BW-1 is ideal for four reasons. (1) Earlier workers established a linear age model for BW-1 based on 24 ^{230}Th dates along the vertical growth axis (Ma et al., 2012). The sample contains banding that is corroborated as annual by the ^{230}Th dating. (2) Given its average growth rate (76 µm/yr) and the 10 µm resolution at the Wisconsin Secondary Ion Mass Spectrometer Laboratory (WiscSIMS), it is possible to make several $\delta^{18}O$ analyses in most annual bands. (3) Drill sample measurements of $\delta^{18}O$ in BW-1 show a large, rapid change across the Younger Dryas (YD)–Holocene transition (at 11.53 k.y. before present; Ma et al., 2012). (4) The cave is near the northern extent of monsoon influence, where the $\delta^{18}O$ value of EASM rainfall likely correlates with summer rainfall amount (Liu et al., 2014).

METHODS

The WiscSIMS ion microprobe is capable of high-precision (±0.3‰ 2 standard deviation [s.d.].) and accurate *in-situ* $\delta^{18}O$ measurements in 10-µm-diameter spots in speleothem calcite (Kita et al., 2009; Orland et al., 2009). Analysis of BW-1 was completed using a standard-sample–standard bracketing technique. Two groups of ~4 analyses of calcite standard UWC-3 ($\delta^{18}O$ = 12.49‰, Vienna standard mean ocean water; Kozdon et al., 2009) bracket each set of 10–15 sample analyses. The 2 s.d. of the bracketing standards represents the spot to spot reproducibility of the intervening samples. (See the GSA Data Repository[1] for detailed results.) Screening based on pit condition and ionization yield (see the Data Repository) removed 77 of the original $\delta^{18}O$ analyses (6%) from the plots and discussion presented here.

Each sample analysis was positioned based on reflected light and confocal laser fluorescent microscope (CLFM) imaging. Prior work demonstrates that CLFM imaging and ion

*E-mail: ijorland@umn.edu

[1]GSA Data Repository item 2015193, supplementary information including data tables, figures, and supplementary description of methods, is available online at www.geosociety.org/pubs/ft2015.htm, or on request from editing@geosociety.org or Documents Secretary, GSA, P.O. Box 9140, Boulder, CO 80301, USA

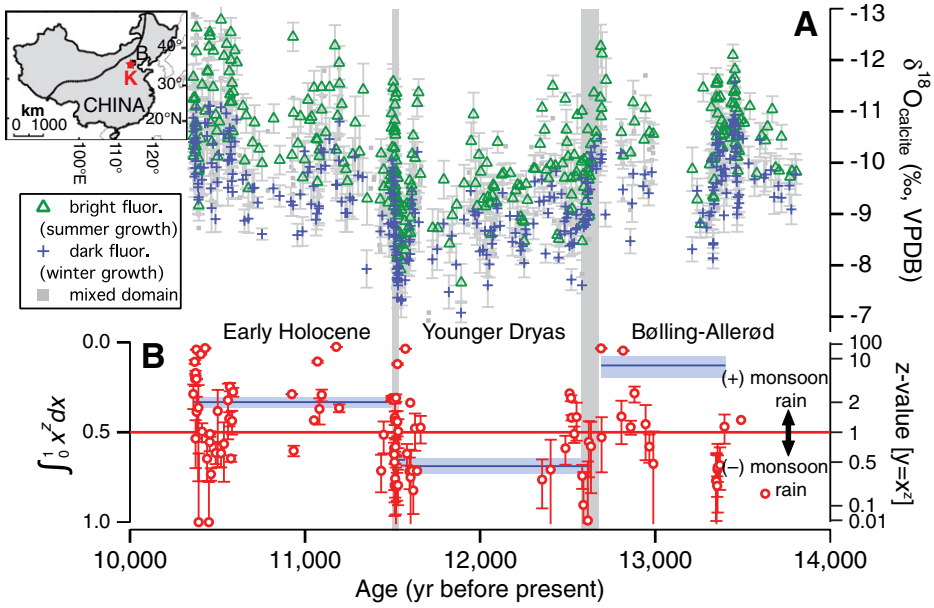

Figure 1. Seasonal resolution $\delta^{18}O$ analyses and intraband variability across stalagmite BW-1 from Kulishu Cave (northeastern China). Inset: Location of Kulishu Cave (K) near Beijing (B). Dashed line indicates the northern extent of modern summer monsoon influence. Modified from Ma et al. (2012). A: Values of $\delta^{18}O$ (Vienna Peedee belemnite, VPDB) categorized by calcite fluorescence (fluor.) and inferred season of growth. Error bars show 2 standard deviations reproducibility. B: Right axis (nonlinear scale) shows the exponent (z value) of a power function with best fit to normalized, intraband $\delta^{18}O$ change in bands with three or more analyses (n = 98; 61 bands have 5 or more analyses). Error bars are 2σ of best-fit residuals for bands with four or more analyses. Left axis (linear scale) indicates the resulting integral of each best-fit power function. Horizontal lines show weighted-average (solid blue; see text) z values with weighted 2σ ranges for four periods discussed in text. Axes in B are oriented so up corresponds to greater annual proportion of monsoon rainfall. Ages are before present, A.D. 1950.

microprobe analysis can be combined to identify annual banding and quantify seasonal geochemical signals in speleothems (Orland et al., 2009, 2012, 2014).

RESULTS

Figure 1 plots 1120 ion microprobe $\delta^{18}O$ values. CLFM imaging reveals distinct annual growth bands throughout the stalagmite (see the Data Repository). The fluorescence of each band follows the same general pattern, with a sharp fluorescent onset followed by a more gradual transition to nonfluorescence. This is the same pattern described in samples from Soreq Cave (Israel), where there is a strong seasonal rainfall gradient (Orland et al., 2009). The fluorescence of each analysis location is classified in Figure 1A, with bright and dark classifications only assigned to spots in the brightest or darkest portions of fluorescent bands. As in Soreq Cave, the bright spot at the beginning of each band consistently has a lower $\delta^{18}O$ value than the dark spot at the end.

Ion microprobe measurements have a 6.0‰ range, from –12.9‰ to –6.9‰ (Vienna Peedee belemnite, VPDB). Analyses were placed in pairs at the beginning and end of 304 annual bands. The variable $\Delta^{18}O_{d\text{-}b}$ (d—dark; b—bright) referenced here and calculated as the $\delta^{18}O$ gradient within an individual band (Orland et al., 2009),

$$\Delta^{18}O_{d\text{-}b} = \delta^{18}O_d - \delta^{18}O_b, \quad (1)$$

has a maximum value of 2.8‰ and an average value of 0.9‰ (n = 304; see the Data Repository).

DISCUSSION

We interpret the $\delta^{18}O$ variability measured across BW-1 and within annual bands as reflecting relative changes in the $\delta^{18}O$ of cave drip waters; prior work found that $\delta^{18}O$ values in BW-1 reflect isotopic equilibrium based on a Hendy test of four horizontal bands (Ma et al., 2012). The hypotheses we test designate EASM rainfall as having a low $\delta^{18}O$ value, which reflects seasonally averaged observations of modern rainfall from a nearby location (see the Data Repository). We note that $\Delta^{18}O_{d\text{-}b}$ values in BW-1 corroborate the seasonally averaged $\delta^{18}O$(rain) observations, implying that the $\delta^{18}O$(rain) signal is attenuated in the overlying karst. Given that the majority of modern annual rainfall occurs during the summer monsoon, we assume that the bright onset of each band, where $\delta^{18}O$(calcite) is at its lowest, records drip waters fed by the onset of the annual EASM. It follows that the dark portion reflects higher $\delta^{18}O$ values of winter and spring drip waters. We also assume that seasonal variation of speleothem growth rate is relatively consistent. With these assumptions in mind, we test the two explanations outlined above for how $\delta^{18}O$ variability in Chinese speleothems is influenced by the EASM.

Each explanation predicts a distinct pattern of seasonal BW-1 $\delta^{18}O$ variability. The Wang-Cheng interpretation predicts that the annual proportion of low-$\delta^{18}O$ (monsoon season) calcite should be higher during the early Holocene and Bølling-Allerød (BA) than during the YD. The Yuan interpretation predicts that the summer monsoon portion of each band will have a consistent annual proportion and will have a lower $\delta^{18}O$ value during the early Holocene and BA versus the YD.

Evidence for Upstream Influence on Rainfall $\delta^{18}O$

Figure 2A plots our $\delta^{18}O$ analyses across the YD-Holocene transition. The earlier drill sampling study (Ma et al., 2012) measured a 2.2‰ decrease in $\delta^{18}O$ across 6 spots and concluded that a shift to a stronger EASM in the early Holocene took ≤38 yr. WiscSIMS measurements of $\delta^{18}O$ (n = 148) in 33 consecutive annual bands indicate that the $\delta^{18}O$ transition took less than half of that time; the full magnitude of the transition occurred in 14 yr for $\delta^{18}O_b$ values and 16 yr for $\delta^{18}O_d$ values. This rate of change is consistent with other annually resolved proxy records for atmospheric reorganization at the end of the YD (Alley et al., 1993; Taylor et al., 1997; Orland et al., 2012).

The seasonal resolution $\delta^{18}O$ profile across the YD-Holocene boundary also tests the two mixing model–based hypotheses described here. Figure 2A shows that summer rainfall $\delta^{18}O$ decreases across the YD-Holocene transition. This observation supports the interpreta-

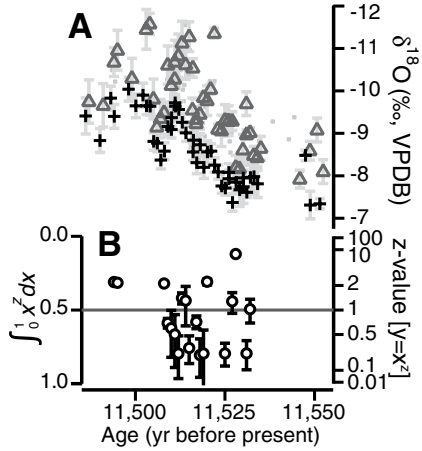

Figure 2. Ion microprobe analysis of $\delta^{18}O$ across the end of the Younger Dryas in stalagmite BW-1 (from northeastern China). The relative ages of data from this 95 yr section are assigned by band counting and corroborated by bracketing ^{230}Th dates (yr before present, A.D. 1950). Symbols and axes as in Figure 1. VPDB—Vienna Peedee belemnite.

tion of upstream Rayleigh-type fractionation (Yuan interpretation), but does not rule out the annual proportion interpretation (Wang-Cheng interpretation), as we show in the following.

Measuring Annual Monsoon Strength

The seasonal resolution of the ion microprobe allows us to investigate the pattern of $\delta^{18}O$ variability within individual annual bands. As described here, $\delta^{18}O$ values in each annual band consistently increase from the summer monsoon season into winter and on into spring. Systematic permutations of this pattern are apparent in different portions of BW-1; $\delta^{18}O$ increases near the beginning of some bands, but near the end of others. In order to illustrate these empirical differences we use a best-fit power function ($\delta^{18}O = \text{distance}^z$) to define a single variable, the exponent z, that describes the shape of $\delta^{18}O$ change within a band. In every band where there are three or more analyses including both a bright and dark spot, the power function is fit to a normalized profile of $\delta^{18}O$ between the first and last spots (Figs. 1B and 2B). The data are normalized such that (distance, $\delta^{18}O$) is (0,0) for each bright spot and (1,1) for each dark spot.

In bands with $z > 1$, $\delta^{18}O$ values increase near the end of the band (Fig. 3). For bands with $z < 1$, $\delta^{18}O$ values increase nearer the beginning. We interpret the shape of $\delta^{18}O$ variability as an indicator of the annual proportion of low $\delta^{18}O$ EASM rainfall, where higher z values represent a larger annual proportion of EASM rainfall. It is possible that higher z values reflect increased summer growth rates, but the variables most likely to cause such a change are themselves dependent on increased rainfall: increased drip water supply, increased soil CO_2 from plant respiration.

The z values suggest that the annual proportion of EASM rainfall was greater during the BA and early Holocene than during the cooler YD. The year-to-year variability in z values is expected; just as with modern weather, a representative climate is determined by averaging over time. Figures 1B and 3A illustrate that weighted average z values of bands with four or more analyses (see the Data Repository) are higher during the BA and early Holocene versus the YD. Thus, the intra-annual variability of $\delta^{18}O$ in BW-1 is consistent with the interpretation that drill sample analyses with relatively low $\delta^{18}O$ values reflect, on average, a larger annual proportion of EASM rainfall, as envisioned in the Wang-Cheng interpretation. It is notable that across the YD-Holocene transition where an abrupt decrease in $\delta^{18}O$ values suggests a rapid atmospheric change, a corresponding change to higher z values is less clear. This suggests that the regional summer monsoon strengthened stochastically during the transition into the Holocene.

In addition to identifying two climatic components of the speleothem $\delta^{18}O$ record that are lost by drill sampling, the ion microprobe data allow us to determine the relative effects of (1) the annual proportion of EASM rainfall, and (2) the $\delta^{18}O$ value of EASM rainfall on the drill sample $\delta^{18}O$ record. For example, at the YD-Holocene transition, we can approximate the bulk $\delta^{18}O$(calcite) of an annual band ($\delta^{18}O_{band}$) from the ion microprobe data:

$$\delta^{18}O_{band} = \delta^{18}O_b + \left(\Delta^{18}O_{d\text{-}b} \times \int_0^1 x^z\,dx\right),$$

where $\Delta^{18}O_{d\text{-}b}$ is from Equation 1 and $\int_0^1 x^z\,dx$ is the integral of the best-fit power function. From the YD into the early Holocene, the average $\delta^{18}O_{band}$ value decreases 1.6‰ while the average $\delta^{18}O_{bright}$ value (EASM season growth) decreases only 1.2‰. This difference suggests that the greater annual proportion of EASM rainfall during the early Holocene contributed to, on average, 25% of the decrease in drill sample $\delta^{18}O$ across the YD-Holocene transition.

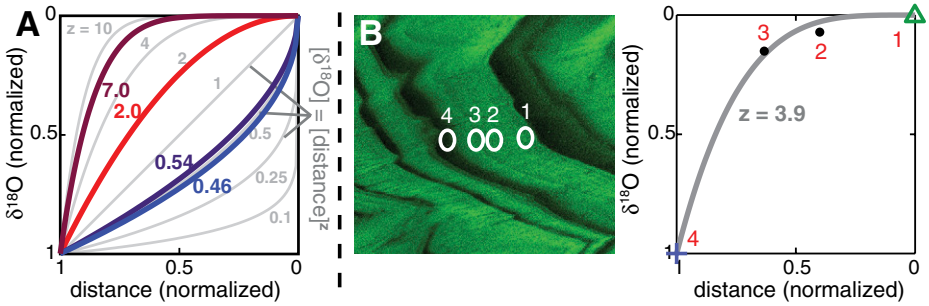

Figure 3. A: Best-fit power functions of normalized intraband $\delta^{18}O$ variability in stalagmite BW-1 (from northeastern China). Axes are normalized to show the pattern of increasing $\delta^{18}O$ values measured between the first (distance = 0) and last (distance = 1) analysis in each annual band. Axis directions match Figures 1 and 2. Colored lines in A illustrate the weighted-average z values measured in four time periods: Bølling-Allerød (z = 7.1, maroon), Younger Dryas (0.46, blue), end of the Younger Dryas (0.54, purple), and early Holocene (2.0, red). B: Fluorescent image and best-fit power curve for one band (growth direction is right to left). The 10 µm analysis spots are labeled 1–4 in both the image and plot. Field of view is 180 µm.

Multifaceted $\delta^{18}O$ Signal in BW-1

A recent isotope-enabled model suggests that changes in the $\delta^{18}O$ of annual precipitation in China are driven exclusively by fractionation of water vapor originating from the "upstream" Indian Ocean (Pausata et al., 2011), with no effect from Pacific moisture sources. That model predicts the $\delta^{18}O$ value of annual precipitation at Kulishu Cave to be 0.5‰–1.0‰ higher for Heinrich Event 1 conditions (triggered by a freshwater pulse in the North Atlantic akin to the YD). The relative increase of modeled $\delta^{18}O$ values purportedly results from decreased rainfall over India. Less rainout over India causes the $\delta^{18}O$ of Chinese precipitation to increase with no effect on rainfall amount in eastern China. By assuming a similar difference between YD and Holocene conditions and accounting for the influence of temperature on speleothem $\delta^{18}O$, we can compare the model results to annually averaged $\delta^{18}O$(calcite) measured across the YD-Holocene transition in BW-1. Given a 1.5 °C warming (Shakun et al., 2012) from the YD into the early Holocene, the 1.6‰ decrease in average $\delta^{18}O_{band}$ values from BW-1 reflects a 1.3‰ decrease in the $\delta^{18}O$ of annual precipitation above Kulishu (fractionation equation from Tremaine et al., 2011), larger than the modeled decrease of 0.5‰–1.0‰ (Pausata et al., 2011). This difference may be due to an upstream effect on Pacific-sourced rainfall, which is insignificant in the Pausata et al. (2011) model. In an earlier model, Zhang and Dellworth (2005) found an early Holocene increase in precipitation over the Philippine Sea, an area of the Pacific that is within the primary source region of EASM rainfall (Liu et al., 2014). Such an increase in precipitation would further lower the $\delta^{18}O$ value of early Holocene rainfall over China. We infer that the Pausata et al. (2011) model erroneously neglects changes in the portion of the monsoon sourced from the Pacific that could contribute to changes in both the seasonal amount and $\delta^{18}O$ value of monsoon rainfall in China. The most recent isotope-enabled model of the modern EASM supports the interpretation that annual rainfall $\delta^{18}O$ reflects a combination of upstream effects and the amount of monsoon rainfall, particularly in northern China (Liu et al., 2014).

Recent satellite observations highlight the influence of the seasonal jet stream position on the amount and source of EASM precipitation (Schiemann et al., 2009; Molnar et al., 2010). In particular, the low $\delta^{18}O$, high-volume summer monsoon precipitation takes place when the jet stream reaches a seasonal position north of the Tibetan Plateau (see the Data Repository). In this context, the reduced proportion of low $\delta^{18}O$ calcite that we observe in the annual bands of BW-1 during the YD could be caused by the jet stream spending less time in its summer position to the north of the Tibetan Plateau than during the early Holocene and BA.

CONCLUSIONS

The seasonal resolution $\delta^{18}O$ data in stalagmite BW-1 reconcile two hypotheses, previously untested in speleothems, that explain variability in Chinese speleothem $\delta^{18}O$. For BW-1, each hypothesis explains a major component of the $\delta^{18}O$ record. The primary component is the absolute $\delta^{18}O$ value of seasonal rainwater, which likely responds to changes in the integrated amount of rainout from tropically sourced water vapor to Chinese cave sites, confirming the Yuan interpretation. We find that a recent model of upstream rainout (Pausata et al., 2011) underestimates the observed change in rainfall $\delta^{18}O$ over northeast China, likely because the model discounts the Pacific Ocean moisture source. We infer that both Pacific and Indian Ocean moisture sources contribute to the $\delta^{18}O$ signal, consistent with the findings of Liu et al. (2014).

The second component of the BW-1 $\delta^{18}O$ record is the annual proportion of low $\delta^{18}O$ summer monsoon rainfall, which confirms the Wang-Cheng interpretation. Intra-annual patterns of $\delta^{18}O$ variability in BW-1 indicate that the average annual proportion of low $\delta^{18}O$ monsoon rainfall during relatively warm periods (BA and early Holocene) is higher than during cold periods (YD). It is likely that $\delta^{18}O$ records from other Chinese speleothems respond to similar effects and that analyzing them at seasonal resolution could reveal both regional- and hemisphere-scale climate changes.

ACKNOWLEDGMENTS

We thank K. Kitajima and D. Nakashima for support at WiscSIMS; B. Hess for sample preparation; and three anonymous reviewers. Imaging was completed at the University Imaging Centers (University of Minnesota), the W.M. Keck Laboratory for Biological Imaging (University of Wisconsin), and the Department of Geoscience Scanning Electron Microscope Laboratory (University of Wisconsin). This manuscript is based on work supported by National Science Foundation (NSF) awards AGS-1231155 and 1103403, and Natural Science Foundation of China award 41230524. WiscSIMS is partly supported by the NSF (grants EAR-03-19230, EAR-10-53466, and EAR-13-55590).

REFERENCES CITED

Alley, R.B., et al., 1993, Abrupt increase in Greenland snow accumulation at the end of the Younger Dryas event: Nature, v. 362, p. 527–529, doi:10.1038/362527a0.

Cheng, H., Edwards, R.L., Broecker, W.S., Denton, G.H., Kong, X., Wang, Y., Zhang, R., and Wang, X., 2009, Ice age terminations: Science, v. 326, p. 248–252, doi:10.1126/science.1177840.

Cheng, H., Sinha, A., Wang, X., Cruz, F.W., and Edwards, R.L., 2012a, The global paleomonsoon as seen through speleothem records from Asia and the Americas: Climate Dynamics, v. 39, p. 1045–1062, doi:10.1007/s00382-012-1363-7.

Cheng, H., Zhang, P.Z., Spötl, C., Edwards, R.L., Cai, Y.J., Zhang, D.Z., Sang, W.C., Tan, M., and An, Z.S., 2012b, The climatic cyclicity in semiarid-arid Central Asia over the past 500,000 years: Geophysical Research Letters, v. 39, L01705, doi:10.1029/2011GL050202.

Dykoski, C., Edwards, R.L., Cheng, H., Yuan, D., Cai, Y., Zhang, M., Lin, Y., Qing, J., An, Z., and Revenaugh, J., 2005, A high-resolution, absolute-dated Holocene and deglacial Asian monsoon record from Dongge Cave, China: Earth and Planetary Science Letters, v. 233, p. 71–86, doi:10.1016/j.epsl.2005.01.036.

Kelly, M.J., Edwards, R.L., Cheng, H., Yuan, D., Cai, Y., Zhang, M., Lin, Y., and An, Z., 2006, High resolution characterization of the Asian Monsoon between 146,000 and 99,000 years B.P. from Dongge Cave, China and global correlation of events surrounding Termination II: Palaeogeography, Palaeoclimatology, Palaeoecology, v. 236, p. 20–38, doi:10.1016/j.palaeo.2005.11.042.

Kita, N.T., Ushikubo, T., Fu, B., and Valley, J.W., 2009, High precision SIMS oxygen isotope analysis and the effect of sample topography: Chemical Geology, v. 264, p. 43–57, doi:10.1016/j.chemgeo.2009.02.012.

Kozdon, R., Ushikubo, T., Kita, N.T., Spicuzza, M., and Valley, J.W., 2009, Intratest oxygen isotope variability in the planktonic foraminifer *N. pachyderma*: Real vs. apparent vital effects by ion microprobe: Chemical Geology, v. 258, p. 327–337, doi:10.1016/j.chemgeo.2008.10.032.

Liu, Z., et al., 2014, Chinese cave records and the East Asia Summer Monsoon: Quaternary Science Reviews, v. 83, p. 115–128, doi:10.1016/j.quascirev.2013.10.021.

Ma, Z.-B., Cheng, H., Tan, M., Edwards, R.L., Li, H.-C., You, C.-F., Duan, W.-H., Wang, X., and Kelly, M.J., 2012, Timing and structure of the Younger Dryas event in northern China: Quaternary Science Reviews, v. 41, p. 83–93, doi:10.1016/j.quascirev.2012.03.006.

Molnar, P., Boos, W.R., and Battisti, D.S., 2010, Orographic controls on climate and paleoclimate of Asia: Thermal and mechanical roles for the Tibetan Plateau: Annual Review of Earth and Planetary Sciences, v. 38, p. 77–102, doi:10.1146/annurev-earth-040809-152456.

Orland, I.J., Bar-Matthews, M., Kita, N.T., Ayalon, A., Matthews, A., and Valley, J.W., 2009, Climate deterioration in the Eastern Mediterranean as revealed by ion microprobe analysis of a speleothem that grew from 2.2 to 0.9 ka in Soreq Cave, Israel: Quaternary Research, v. 71, p. 27–35, doi:10.1016/j.yqres.2008.08.005.

Orland, I.J., Bar-Matthews, M., Ayalon, A., Matthews, A., Kozdon, R., Ushikubo, T., and Valley, J.W., 2012, Seasonal resolution of Eastern Mediterranean climate change since 34 ka from a Soreq Cave speleothem: Geochimica et Cosmochimica Acta, v. 89, p. 240–255, doi:10.1016/j.gca.2012.04.035.

Orland, I.J., Burstyn, Y., Bar-Matthews, M., Kozdon, R., Ayalon, A., Matthews, A., and Valley, J.W., 2014, Seasonal climate signals (1990–2008) in a modern Soreq Cave stalagmite as revealed by high-resolution geochemical analysis: Chemical Geology, v. 363, p. 322–333, doi:10.1016/j.chemgeo.2013.11.011.

Pausata, F.S.R., Battisti, D.S., Nisancioglu, K.H., and Bitz, C.M., 2011, Chinese stalagmite $\delta^{18}O$ controlled by changes in the Indian monsoon during a simulated Heinrich event: Nature Geoscience, v. 4, p. 474–480, doi:10.1038/ngeo1169.

Schiemann, R., Lüthi, D., and Schär, C., 2009, Seasonality and interannual variability of the Westerly Jet in the Tibetan Plateau region: Journal of Climate, v. 22, p. 2940–2957, doi:10.1175/2008JCLI2625.1.

Shakun, J.D., Clark, P.U., He, F., Marcott, S., Mix, A.C., Liu, Z., Otto-Bliesner, B., Schmittner, A., and Bard, E., 2012, Global warming preceded by increasing carbon dioxide concentrations during the last deglaciation: Nature, v. 484, p. 49–54, doi:10.1038/nature10915.

Taylor, K.C., et al., 1997, The Holocene–Younger Dryas transition recorded at Summit, Greenland: Science, v. 278, p. 825–827, doi:10.1126/science.278.5339.825.

Tremaine, D.M., Froelich, P.N., and Wang, Y., 2011, Speleothem calcite farmed in situ: Modern calibration of $\delta^{18}O$ and $\delta^{13}C$ paleoclimate proxies in a continuously-monitored natural cave system: Geochimica et Cosmochimica Acta, v. 75, p. 4929–4950, doi:10.1016/j.gca.2011.06.005.

Wang, Y.J., Cheng, H., Edwards, R.L., An, Z.S., Wu, J.Y., Shen, C.C., and Dorale, J.A., 2001, A high-resolution absolute-dated late Pleistocene monsoon record from Hulu Cave, China: Science, v. 294, p. 2345–2348, doi:10.1126/science.1064618.

Wang, Y.J., Cheng, H., Edwards, R.L., Kong, X., Shao, X., Chen, S., Wu, J., Jiang, X., Wang, X., and An, Z., 2008, Millennial- and orbital-scale changes in the East Asian monsoon over the past 224,000 years: Nature, v. 451, p. 1090–1093, doi:10.1038/nature06692.

Yuan, D., et al., 2004, Timing, duration and transitions of the Last Interglacial Asian Monsoon: Science, v. 304, p. 575–578, doi:10.1126/science.1091220.

Zhang, R., and Dellworth, T.L., 2005, Simulated tropical response to a substantial weakening of the Atlantic: Journal of Climate, v. 18, p. 1853–1860, doi:10.1175/JCLI3460.1.

Manuscript received 12 January 2015
Revised manuscript received 9 April 2015
Manuscript accepted 15 April 2015

Printed in USA

Geology

Direct measurements of deglacial monsoon strength in a Chinese stalagmite

Ian J. Orland, R. Lawrence Edwards, Hai Cheng, Reinhard Kozdon, Mellissa Cross and John W. Valley

Geology 2015;43;555-558
doi: 10.1130/G36612.1

Notes